Crystallization evolution of accessory minerals in palaeoproterozoic granites of Bastar Craton, India

Dinesh Pandit*

Department of Geology, Centre of Advanced Study, Institute of Science, Banaras Hindu University, Varanasi 221 005, India

The Malanjkhand and Dongargarh granitoids are compared to study the role of accessory minerals (apatite, zircon, titanite and titanomagnetite) to understand crystallization evolution of Palaeoproterozoic granitic magmatism in the Bastar Craton, central India. Two varieties of titanite (magmatic and hydrothermal types) are observed in the Palaeoproterozoic granitoids. Occurrence of zircon, apatite, titanite and titanomagnetite as accessory phases in the Palaeoproterozoic granitoids indicates that the early stage of crystallization of granitic magma was saturated with Zr, P and Ti. Petrography and mineral equilibria reaction suggest that magmatic titanite in the Palaeoproterozoic granitoids was formed due to hydration of amphiboles and biotites which favours high $f\,O_2$ and $f\,H_2O$ conditions. Apatite composition suggests that it was formed in the granitic magma at nearliquidus to near-solidus temperature (900–1000°C) which increased fugacity ratio $\log(f_{H_2O}/f_{HF})$ and also controlled the halogen budget during magma crystallization. Relatively high halogen content in the apatites from the Malanjkhand Granitoid (MG) indicates that the parental magma was enriched in F and Cl compared to Dongargarh Granitoids (DG), implying a dominant role of halogens in metal transportation and hydrothermal mineralization. In MG, apatite was the earliest phase to be crystallized in granitic magma followed by zircon and titanite whereas, in DG, crystallization of zircon was followed by apatite and titanite. Two contemporaneous plutons, DG and MG, represent a unique Palaeoproterozoic granitic magmatism wherein early progressive crystallization is dominated by accessory mineral saturation in a relatively static environment with constant magma composition.

Keywords: Accessory minerals, Bastar Craton, Dongargarh, granite, Malanjkhand.

THE most common accessory minerals which occur in granitic rocks include titanite, apatite, zircon, rutile and monazite, which are regarded as petrogenetic indicators of early stage of crystallization of granitic magma[1–6]. These minerals preserve the most significant records of magmatic evolution (i.e. generation, segregation, ascent and emplacement) and crystallization history of granitoids (i.e. dissolution, substitution and replacement). Mineral chemistry of these phases helps to constrain various important physico-chemical parameters during their crystallization evolution. The modal abundance of these minerals is less than 1% in granitoids, but their presence in magma may have significant roles upon distribution of various trace elements, rare earth elements (REE) and radiogenic isotopes[1]. The crystal structures of apatite and titanite as accessory minerals are suited for incorporation of trace elements and REE along with halogens during crystallization of granitic magma[7–9]. Zircon, rutile, apatite and monazite are particularly suited for geochronologic applications because they contain elements having properties like radioactivity, physicochemical durability and resistance to diffusion re-equilibration[10]. Enrichment of trace elements in accessory minerals crystallized from fractionating magma or as residual minerals mostly depended on their bulk concentrations in the granitic magma that underwent partial melting[1,3]. Titanite occurs as accessory mineral in granitoids, and is also found in a wide range of geological environments and also occurs in mafic rocks[11]. Even though experimental studies suggested that titanites are mostly crystallized from magma at an early stage[1,12], there are evidences of occurrences of secondary titanites in granitoids from the Tribec Mountains, Slovakia[13], metamorphic terranes of amphibolites-facies metapelite rocks[14], shear zone from Carthage-Colton, Adirondack Mountains, New York, USA[15], and ultra-high pressure rock from Kokchetav Massif, Kazakhstan[16]. The coupled substitution of Al and F for Ti and O respectively can lead to titanite deviating from its ideal composition[9]. For example, Al–OH bearing titanite most probably formed due to decomposition of biotite in low-temperature geological environments by Al + OH $\leftrightarrow$ Ti + O substitution mechanism[11].

The aim of this study is to understand the role of accessory minerals such as titanite, titanomagnetite and apatite in the evolution of Palaeoproterozoic granitic magmatism in the Bastar Craton of the Indian Subcontinent. The objective is divided into three parts: (1) petrographic and mineralogical studies of accessory minerals (zircon, apatite and titanite); (2) estimating the pressure–temperature

*e-mail: dpandit@hotmail.com
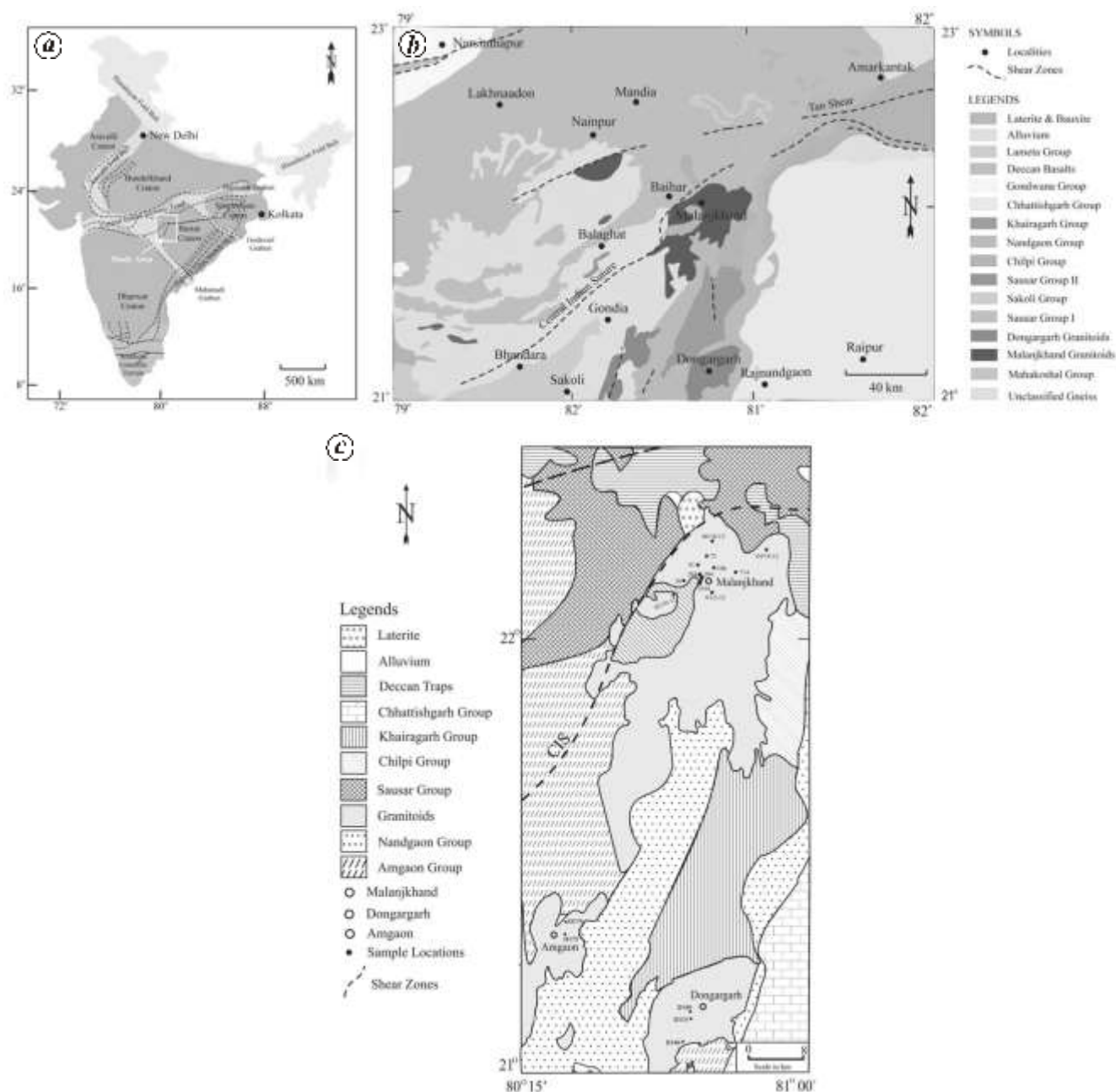
Figure 1. *a*, Study area adjacent of the Central Indian Tectonic Zone in the map of India; *b*, Regional scale geological map of northern Bastar Craton; *c*, Geological map of Malanjkhand and Dongargarh granitoids showing the sample locations (modified after Jain *et al.*[87]; Neogi *et al.*[21]).

conditions of crystallization of granitic magma from accessory minerals; and (3) studying the crystallization evolution of titanite, zircon, apatite and post-magmatic involvement of hydrothermal processes.

Geological and tectonic settings

The Precambrian shield of Central India is dominantly occupied by the continental block of Bastar Craton[17] and ENE–WSW trending Central Indian Tectonic Zone (CITZ) (Figure 1 *a*). CITZ comprises two parallel struc-

tural domains: Son–Narmada (SONA) lineament in the north and Sausar Mobile Belt (SMB) in the south. Southern boundary of CITZ is known as the Central Indian Suture (CIS)[18,19]. The geology of Bastar Craton comprises various litho-units ranging from Early Archean (granite gneisses) to Proterozoic (Malanjkhand and Dongargarh granitoids and its equivalent) in age and preserves a record of several episodes of Precambrian orogenic cycles and metamorphic tectonomagmatic episodes. The Bastar Craton contains three major supracrustal sequences, i.e. the Kotri–Dongargarh, the Sakoli and the Sausar

Supergroup. The Kotri–Dongargarh Supergroup[20] is composed of two litho groups, viz. Nandgaon Group dominated by rhyolites with subordinate occurrences of dacites, andesites and basalts[21], and the Khairagarh Group which unconformably overlies the Nandgaon Group and consists of volcano-sedimentary sequences of shales and sand-stones[22–25]. Subsequently, the stratigraphy of Kotri–Dongargarh Supergroup has been revised into a single Dongargarh group by Sensarma and Mukhopadhyay[22–24]. The Sakoli Group consists mainly of low grade metamorphic rocks comprising of slate, phyllites, bimodal volcanic suite, schists, metabasalts, cherts, conglomerates and Banded Iron Formation[26]. The Sausar Group comprises polymetamorphic belt component of the regional CITZ and is bounded by granulite belts in the northern and southern side[27]. Numerous intrusive mafic dyke swarms such as Gidam–Tongpal, Bhanupratappur–Keskal, Narainpur-Kondagaon and Bijapur-Sukma swarm, cross-cut various granitoids and supracrustal rocks in the Bastar Craton[28]. The Chhattisgarh and the Indravati Basin are two major Proterozoic basins comprising thick sedimentary sequences of conglomerates, sandstones, shales, limestones, cherts and dolomites[29].

The Malanjkhand and Dongargarh Granitoids are two prominent Paleoproterozoic litho units in the northern part of the Bastar Craton (Figure 1 b). The Malanjkhand Granitoid (MG) is located in proximity to the south of CIS. Three units of granitoids plutons are located further 50–60 km south of MG. These three granitoid batholiths are known as Dongargarh, Amgaon and Dhanora–Manpur plutons. Bimodal volcano-sedimentary sequences of Dongargarh Group separate the MG and DG plutons[22–24]. In MG, late stage hydrothermal activities and deuteric alterations promoted various secondary processes such as saussuritization of feldspar, sericitization of mica, chloritization, epidotization which produced various secondary mineral phases such as chlorite, hydrothermal epidote and titanites[30–37].

Palaeoproterozoic granitic magmatism in Bastar Craton

The area adjoining the southern part of CITZ and western part of Proterozoic Chhattisgarh basin in the central Peninsular India is marked by emplacement of a number of granitoid plutons (Figure 1 b). Among these plutons, Palaeoproterozoic Malanjkhand and two units of Dongargarh plutons have been thoroughly studied[38–41]. Geochemical studies suggest that the Malanjkhand pluton is granite–granodiorite in composition[38,40,41] whereas Dongargarh pluton is strictly a granite[38,40,42]. Kumar et al.[43] and Kumar and Rino[41] proposed that MG originated due to mixing of mafic and felsic magma in various proportions within a dynamic magma chamber and emplaced at shallow crustal level based on field, mineralogical and geochemical evidences. Occurrence of oscillatory zoning in magmatic epidotes reported from MG indicates that there was cyclic change in the oxygen fugacity or bulk composition of granitic magma during crystallization[34]. Late-stage hydrothermal activity following the granite emplacement seems to have operated under identical temperature conditions obtained from binary feldspar geothermometer and the characteristics of aqueous fluid (salinity and homogenization temperature) in both the granitoids seem to be broadly similar[33]. Some petrogenetic aspects of MG including the small leucogranite unit phase have been discussed earlier[44,45]. The Palaeoproterozoic bimodal large igneous province with subequal volumes of nearly coeval felsic–mafic volcanic rocks occurs in the Dongargarh Group of Bastar Craton, which is driven by a common thermal perturbation melting of the crust and mantle in an extensional tectonic setting[46]. Rapid eruption of high temperature Bijli rhyolite in the Palaeoproterozoic bimodal Dongargarh Group indicates decompression melting in an extensional setting[47].

Srivastava[48] also suggested that an intracratonic rift setting was responsible for emplacement of numerous mafic dyke swarms and boninite–norite volcanic suite during Neoarchean–Palaeoproterozoic. Occurrence and geochemistry of boninite dyke indeed demonstrates that Palaeoproterozoic Dongargarh Supergroup represents a fossil subduction zone in the Archean of Bastar Craton[49]. Naganjaneyulu and Santosh[50] considered the Mesoproterozoic event to mark the timing of subductioncollision tectonics along the CITZ after examining various geochronological data. Most recently, Kumar et al.[51] suggested the Paleoproterozoic to Mesoproterozoic time interval for extension of central and Eastern Indian Tectonic Zones.

Petrography

Among accessory minerals, the modal abundance of titanite in granitoid is much higher than that of other mineral phases crystallizing from later residual melt[52]. In this study, the occurrence of two types of titanites (magmatic and hydrothermal titanites) from the Palaeoproterozoic granitoids (MG and DG) in Bastar Craton is being reported for the first time. In MG and DG, titanite occurs in the form of big, stout, euhedral grains measuring up to 1 mm in length. Majority of these titanites are associated with quartz, hornblende, biotite, epidote and plagioclase. Sometimes apatite, zircons and opaque are also present as inclusions within titanite (Figure 2 a–f). This type of titanite shows microtexture similar to that reported from the Ross of Mull Granite, northeastern Scotland and is considered to be of magmatic origin[3,53]. Therefore, such a variety of titanite is referred to as primary or magmatic titanite in this study. Small anhedral lozenge-shaped titanite with irregular grain boundaries is associated with
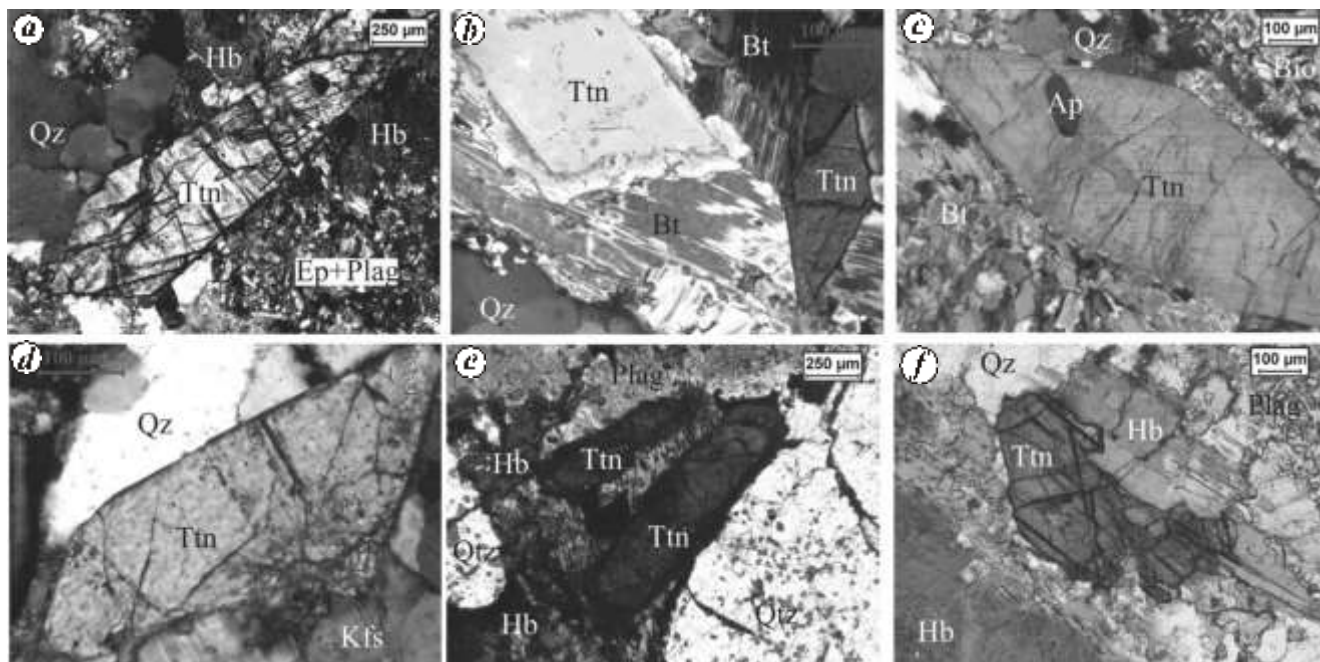
Figure 2. Photomicrographs showing mineral assemblage with magmatic titanite from the MG: *a*, Big stout grains of titanite with quartz + hornblende + plagioclase + epidote; *b*, Euhedral grains of titanite with biotite and quartz; *c*, Lozenge shaped euhedral titanite with apatite with biotite + quartz; *d*, Rhombohedra grain of titanite with quartz + K-feldspar. Representative magmatic titanite from DG shows in (*e*) and (*f*) with hornblende + plagioclase + quartz mineral assemblages.
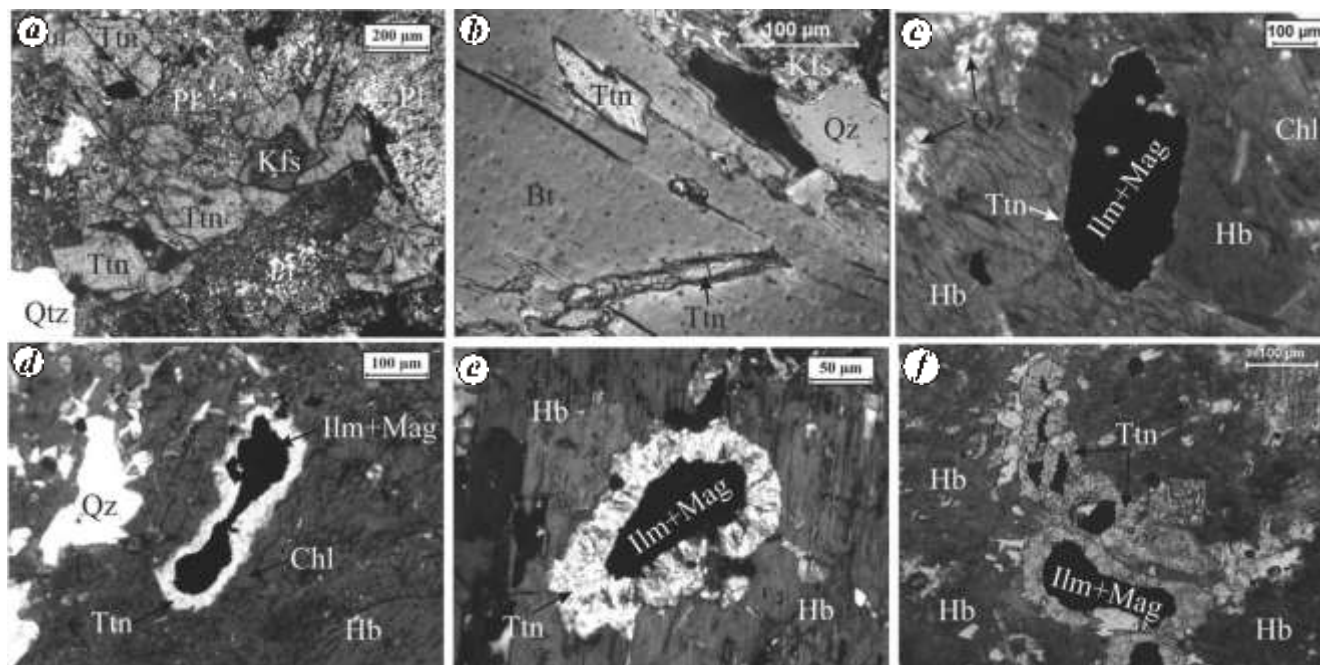
Figure 3. Photomicrographs of hydrothermal titanite from the Malanjkhand granitoid: *a*, Titanite inclusions with altered plagioclase + K-feldspar; *b*, Titanite inclusions in biotite along with quartz. Reaction rims of hydrothermal titanite on titanomagnetite (ilmenite–magnetite composite) grains within chloritized hornblende phenocrysts from the DG as shown in (*c*), (*d*), (*e*) and (*f*).

sassuritized plagioclase (Figure 3 *a*) and chloritized biotite (Figure 3 *b*) in MG. Such titanites are compositionally high in Al–OH content and are most probably of secondary origin[11,54]. Reaction rims of titanite around opaque mineral grains within amphibole are common in DG, which is also one of the characteristic features observed in this granitoid unit (Figure 3 *c–f*). The width of reaction rims varies between 10 and 15 μm. Most of the opaque phases show composite texture of ilmenite–magnetite grains and most probably titanomagnetite. At

few places, it is present as well-grown grains with conspicuous fracturing. The morphology of titanite rims is similar to that reported from four metapelitic and amphibolitic-facies terranes[14] and carboniferous I-type granites/granitoids in the Tribec Mountains, Slovakia[13], where it is considered to be of secondary or hydrothermal origin[3]. This type of titanite is referred to as hydrothermal/secondary titanite in the present study.

BSE images of magmatic titanite from MG show two types of zoning classified as oscillatory zoning without inclusion (Figure 4 *a*) and sector zoning with inclusions of apatite (Figure 4 *b*). Mineral grains with oscillatory zoning show evidence for a cyclic alteration in the chemical composition of discrete growth-shells in micrometres to nanometres thickness and such mineral zoning is a common well-concealed phenomenon in rocks of magmatic origin[55]. Occurrence of sector zoning in mineral grains of intrusive rocks suggests a natural consequence of slow lattice diffusion form of homogeneous disequilibrium[56]. These two types of zoning are caused because of chemical variation within titanite grains, which depends on host rock chemistry and remains unaffected by fluid composition during hydrothermal alteration[8]. Sector zoning in magmatic titanite developed due to magma chamber processes, while oscillatory zoning in titanite is originated due to some localized crystallization processes including nonequilibrium crystal growth and coupled-substitution effects[3]. Most of the magmatic titanites in MG are associated with biotite (Figure 4 *c*), whereas apatite is present as inclusions (Figure 4 *d*). It indicates that primary titanite starts growing after formation of apatite during crystallization of granitic magma. Oscillatory zoning in magmatic titanite indicates cyclic change in magma composition[5] and crystallization of oxidized silicic magma[3]. Zones in titanite grains reflect growth due to changes in melt composition, oxygen fugacity, temperature, rare earth element and high field strength element contents[53,55]. Concentric fine-scale oscillatory zoning and major discontinuities are related to the variation in titanite stability and favoured by mixing processes that include complete mixing of crystal-free melts, crystal transfer between partially crystallized magma and late-stage diffusive exchange within the magma chamber[57].

Titanite occurs as rims around titanomagnetite grains which are clearly observed in photomicrographs obtained from DG (Figure 5 *a*); whereas BSE images of the same titanite rims show relatively weak textural contrast with titanomagnetite grain (Figure 5 *b*). In DG, a large phenocryst of hornblende contains inclusions of titanomagnetite, which are surrounded by titanite rims (Figure 5 *c*). These titanite rims are most probably of secondary or hydrothermal origin. In MG, hydrothermal titanites occur as reaction rims as well as reaction products along conspicuous fracture zones in titanomagnetite grains as observed in the BSE image (Figure 5 *d*). The microtex-

ture and morphology of titanite suggest presence of more than one generation of titanite in both MG and DG. Both magmatic and hydrothermal titanites occur in samples #56 and #714 with relatively less abundance of hydrothermal titanite in samples #01/2–12 from MG.

Apatite grains occur as euhedral, equant to sub-equant, oval or prismatic shaped crystals (Figure 2 *c*) and sometimes found along intergranular spaces between other minerals (Figure 4 *b*). Such apatites are of magmatic origin[10]. They occur mainly in acicular habit and are found as inclusions in biotite (Figure 2 *c, d*), occasionally in plagioclase and hornblende.

Mineral chemistry

Mineral chemical studies of accessory minerals such as titanite, titanomagnetite and apatite were carried out on selected samples from Palaeoproterozoic granitoids to understand the magmatic and hydrothermal processes. These accessory mineral assemblages preserve the crystallization history of igneous rocks and initial records of magma chamber processes[2,57].

Magmatic titanite is a common accessory mineral in granitoid rocks displaying compositional variability because of coupled substitution between Al and F for Ti and O in their respective crystal sites[9]. It is associated with biotites and amphiboles in MG and DG. The magmatic titanite shows significant variation in its major element oxide composition (Supplementary Tables 1 and 2).

In both MG and DG, hydrothermal titanite mostly occurs as inclusions in biotite as well as in hornblende and also in the form of reaction rims around titanomagnetite. It occurs in higher modal abundance along with chloritized biotites in MG as compared to DG. Major element oxides composition of hydrothermal titanites in MG (Supplementary Table 3) and in DG mostly occurs as inclusions in hornblende (Supplementary Table 4) content or not detectable.

Overall, the major element mineral chemistry of two types of titanites in MG is more or less similar with some minor differences. Thus, it is difficult to distinguish between magmatic and hydrothermal titanite based on their major element oxide composition in MG because of extensive deuteric alterations and hydrothermal activities[30,33–37,58,59]. This is because coupled substitution of Al and F for Ti and O in titanite resets their composition during late stage hydrothermal activities thus, overprinting the magmatic composition in MG. However in the case of DG, there are significant differences between magmatic and hydrothermal titanites such as low TiO_2 and CaO with high Al_2O_3 and FeO + MgO. This discrimination is caused because of weak hydrothermal event or activities and restriction to local scale.

The iron-titanium oxides commonly found in igneous rocks and forming three fundamental solid-solution series in FeO, Fe_2O_3, and TiO_2 system are magnetite–ulvospinel
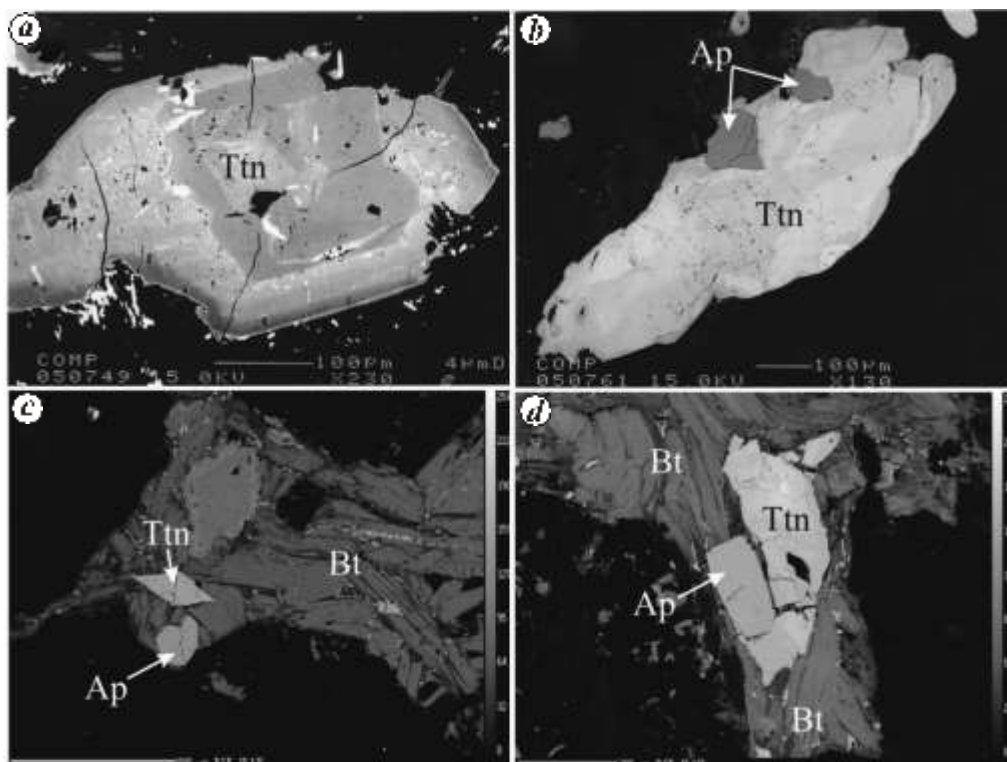
Figure 4. BSC images of magmatic titanite from the Malanjkhand granitoid: *a*, Equant grain with Sector zoning; *b*, Sub-equant grain with inclusions of apatite; *c*, *d*, Biotite host grain in association with titanite and apatite. Mineral abbreviations are according to Whitney and Evans[88].
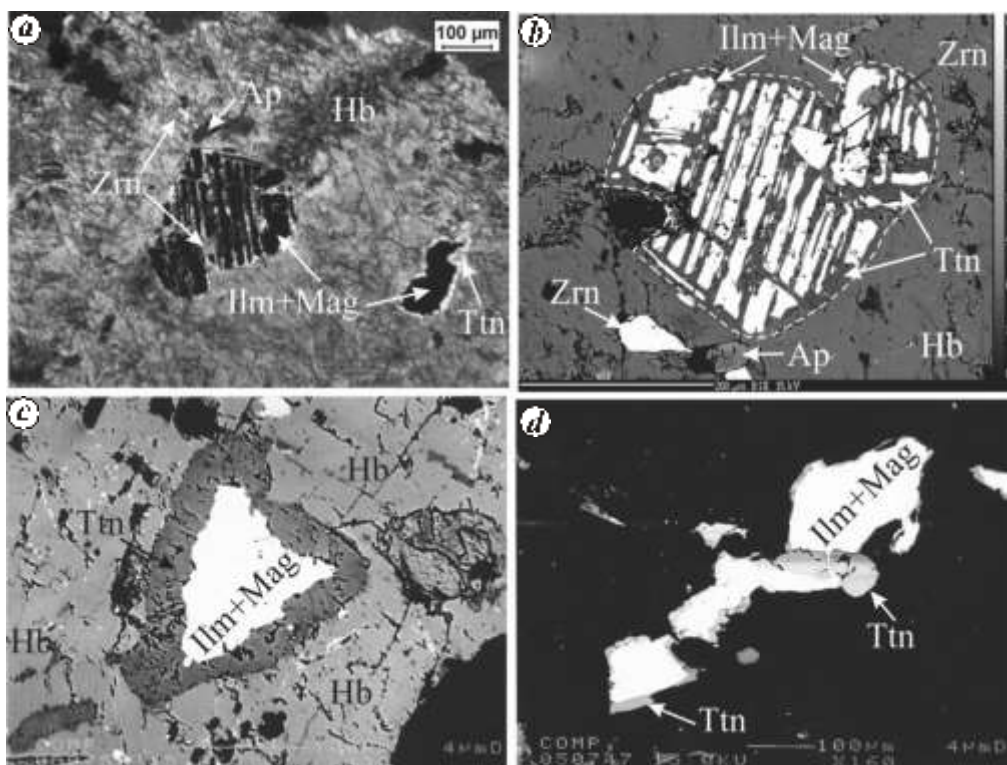
Figure 5. Photomicrographs of hydrothermal titanites from the DG. *a*, Reaction rims of titanite on ilmenite–magnetite composite grains within hornblende phenocrysts and corresponding BSE shown in (*b*) with zircon and apatite as inclusion in hornblende dotted line indicates marked the reaction rim. *c*, BSE images show reaction rim of hydrothermal titanite around titanomagnetite grain hosted in hornblende. *d*, Inclusions of hydrothermal titanite along with ilmenite–magnetite grains. Mineral abbreviations are according to Whitney and Evans[88].

series (titanomagnetite), hematite–ilmenite series (titano-hematite) and pseudobrookite–ferrobrookite series[60].

Hydrothermal titanite occurring as reaction rims around titanomagnetite within amphibole phenocrysts is one of the most common features in DG (Figure 3 c–f) whereas in the case of MG, it occurs as inclusions within biotites (Figure 2 a, b) and sometimes in amphiboles. Mineral analysis of composite grains of ilmenite and magnetite in DG using EPMA reveals that these two occur as separate phases whereas their grain boundaries are difficult to distinguish in photomicrographs (Figure 3 c–f) and BSE images (Figure 5 a–d). The FeO_{tot} and TiO_2 composition in ilmenites from DG ranges from 40.76 to 43.04 wt% and 52.27 to 53.32 wt% respectively (Supplementary Table 5). Significant variation observed in ilmenite composition is perhaps due to relative enrichment in TiO_2 from its ideal value (Figure 7). Magnetite composition is restricted to average FeO_{tot} content of 88.81 wt% (Supplementary Table 6). Mineralogical studies inferred that titanomagnetite is more oxidized and its composition is closer towards titanomaghemite line (Figure 7) because of hydrothermal alteration processes. Amphiboles occur as stout large grains in both MG and DG plutons. Titanite, apatite, zircon and titanomagnetite are frequently observed as inclusions in amphibole grains. Some of these amphiboles are chloritized (Figure 3 c, d) due to hydrothermal alteration processes. Major element oxide compositions of amphiboles are presented in Supplementary Table 7 for both Paleoproterozoic granitoids (MG and DG). The structural formula is calculated based on 23 oxygen atoms per formula unit using NEWAMPHCAL program[61]. Most of the amphibole compositions are restricted between two end member series, pargasite–hornblende and edendite–hornblende. Martin[62] suggested that amphiboles crystallized from parent melts are restite free, whereas high X_{Mg} indicates crustal contamination during crystallization. Amphiboles from MG are free from restite and there is no significant variation in composition, i.e. Al^{IV} varies from 0.91 to 1.0 and X_{Mg} varies from 0.55 to 0.68, which indicates its crystallization from parent melts. However, amphiboles from DG have more variable composition, i.e. Al^{IV} and X_{Mg} range from 1.06 to 1.83 and 0.10 to 0.13 respectively, and occasionally contain restite (Figure 3 c). Higher X_{Mg} in amphiboles indicates higher degree of crustal contamination in parental magma during crystallization in MG compared to DG. Zoning in magmatic titanite and apatite also provide adequate evidences of crustal contamination due to mixing of mafic magma in the Palaeoproterozoic granitoids. Biotites are more abundant in MG as compared to DG, containing inclusions of magmatic (Figure 2 b) and hydrothermal titanites (Figure 3 b) as well as apatites (Figure 4 c, d). Occasionally, zircon also occurs as inclusions in biotite in both Palaeoproterozoic granitoids. Biotites from MG is Mg rich (MgO = 2.55–14.78 wt%) and Fe poor (FeO_{tot} = 17.54–

20.29 wt%); vice versa DG is Mg poor (MgO = 3.91–5.45 wt%) and Fe rich (FeO_{tot} = 25.78–29.26 wt%). A temperature range of 547–602°C for MG and 487–562°C for DG (Supplementary Table 8) is estimated using Ti in biotite geothermometry, which indicates re-equilibration of biotite during alteration processes in both the granitoids. Sample #41, point #15 from MG provides slightly low temperature estimates possibly due to remobilization of excess Ti from biotite during hydrothermal alterations. It is inferred that Ti-substitution in biotite is a function of Mg content and temperature and indicates local departure from equilibrium due to hydrothermal alteration to form chlorite[37,63,64].

Apatites are valuable petrogenetic indicators showing volatile behaviour in mafic as well as felsic igneous rocks. Composition of apatites can be linked with the fugacities of F^-, OH^- and Cl-complexes through exchange equilibria[65]. Mineral composition of apatites from DG and Mg is completely different in terms of CaO and P_2O_5 content (Supplementary Table 9). Apatites in MG show low Ca and high F content in compared to apatites from DG. Variation in the concentration of halogens (F and Cl) in apatites from MG (F = 3.67–6.38 wt% and Cl <0.12 wt%) and DG (F = 1.51–1.86 wt% and Cl <0.02 wt%) is responsible for changes in their fugacity ratios during the crystallization of intrusive granitoids[12]. In MG apatites contain La_2O_3 up to 0.31 wt% and Ce_2O_3 up to 0.92 wt%, whereas in DG, rare earth content in apatite is comparatively lower with La_2O_3 ranging from 0.02 to 0.20 wt%, Ce_2O_3 and Nd_2O_3 ranging from 0.20 to 0.50 wt% and 0.18 to 0.34 wt% respectively (Supplementary Table 9).

Estimated crystallization temperature from apatite-biotite geothermometry[66] for MG ranges from 920°C to 1005°C, whereas most of the biotite in DG have higher value of IV(F) >3.0; thus such compositions are not useful in thermometric calculations. Only in one case (Slide #D175 Point #113), the IV(F) value is 2.482 corresponding to 927°C as apatite crystallization temperature in DG. The apatite–biotite equilibria provide the temperature of partial melting of crustal protoliths at near-liquidus that corresponds to fugacity ratio log(f_{H_2O}/f_{HF}), 3.0–4.0 for MG and >4.0 for DG. It indicates that apatites crystallized from granitic melt, which was produced from partial melting of crustal protolith[66]. Apatites saturated in granitic melt at very low concentrations of P_2O_5 (ref. 67) and therefore are able to concentrate geochemically important rare earth elements[68]. Apatites in MG are strongly zoned and have uniform composition as seen in the BSE images. Oscillatory zones in apatites reflect multi-generation growth during progressive crystallization within magma chamber[69].

Petrogenetic processes and accessory minerals

The accessory mineral assemblages are sensitive to a range of important parameters such as temperature, oxygen

fugacity, melt composition and dissolution history of evolving magma[70–72]. There are clear correlations among accessory mineral occurrences and their textures that indicate variations in physicochemical conditions, which are very useful in constraining igneous processes within the magma chamber. Compositional variability in accessory minerals from the Palaeoproterozoic granitoids in central India bear consequences of variation in melt composition as well as physicochemical condition during late stage hydrothermal processes.

Magmatic titanite

Magmatic titanite is a product of late-stage oxidation during crystallization of granitoid pluton[3]. Constraints from titanite-forming reactions are good indicators of changes in pressure, temperature and oxygen fugacity of granitic magma[71]. Titanite composition depends on the fugacities of oxygen and fluorine. There are a number of mineral phases occurring as inclusions in titanite and genetically, these can be identified as of magmatic and hydrothermal origin. Primary mineral inclusions of apatite, zircon and titanomagnetite occur in titanite crystals in MG and DG. Magmatic titanite most likely formed because of hydration breakdown processes can be explained by the reaction model of Broska *et al.*[13] involving amphibole, K-feldspar, biotite and titanomagnetite as follows

$$7Tr + 2Kfs + 3Titanomagnetite + 3H_2O$$

$$= 3Ttn + 2Phl + Qz, \qquad (1)$$
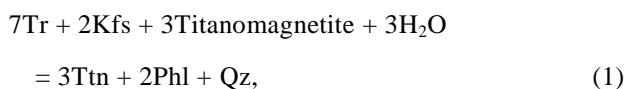
where Tr is tremolite; Kfs, K-feldspar; Ttn, titanite; Phl, phlogopite and Qz, quartz.

Ti-bearing biotite in MG and Ti-enriched magnetite or ilmenite–magnetite composite grains are common in samples collected from DG and both serve as a source of Ti for the formation of titanite. Possibly, there was increase in oxygen and water fugacity that favoured hornblende hydration in granitic magma producing magmatic titanite in both the granitoids.

Hydrothermal titanite

Hydrothermal titanite in samples from MG occurs as finegrained aggregates (~50–100 μm size) replacing magmatic biotite and appears to be coeval with chlorite formation (Figure 2 *a*). It also occurs as small euhedral aggregates in biotite gains (Figure 2 *b*) and is associated with plagioclase and K-feldspar. The equilibrium reaction proposed by Broska *et al.*[13] for the formation of hydrothermal titanite explains its presence in MG, which is as follows

$$Ti\text{-bearing Ann} + An = Ttn + Ep + Chl + Qz, \qquad (2)$$
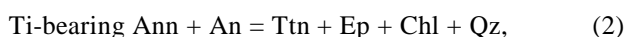
where Ann is annite; An, anorthite; Ep, epidote and Chl, chlorite.

Formation of hydrothermal titanite, especially in case of titanite rims around titanomagnetite in DG, is most likely due to hydration reactions involving amphibole, plagioclase, chlorite and magnetite. The hydration reaction is stabilized in DG at high oxygen (fO_2) and water (f_{H_2O}) fugacity due to late stage hydrothermal activities with internal evolution of the exsolved fluid[33]. It can be explained by the following equilibrium reaction

$$6Fprg + 12Ilm + 4O_2 + 6H_2O$$

$$= 12Ttn + 6Ab + 3Fe\text{-Ame} + 8Mag, \qquad (3)$$
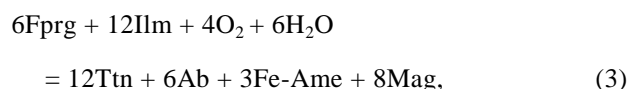
where Fprg is ferropargasite; Ilm, ilmenite; Ab, albite; Ame, amesite and Mag, magnetite.

Ilmenite–magnetite equilibria

Ilmenite and magnetite occur together as composite grains within hornblende in DG. Ilmenite–magnetite composite grains are formed due to subsequent unmixing via oxidation of the ulvospinel (Usp)[61]. This can be expressed by the following equilibrium reaction

$$6Usp = 6Ilm + 2Mag + O_2. \qquad (4)$$
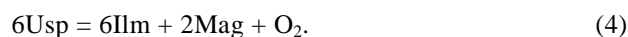
This reaction suggests that in DG, Fe–Ti oxides reequilibrate at subsolidus conditions; however, ilmenite and magnetite may or may not change in their composition during cooling of granitic magma. The titanite + magnetite + quartz assemblage in DG is helpful in temperature-oxygen fugacity estimation for granitic magma[71]. The estimated values of oxygen fugacity in DG are very close to FMQ buffer (Figure 6).

Amphibole geobarometry

Presence of amphiboles in granitoids is critical for deciphering the crystallization pressure and emplacement depths of granitic magma. Amphibole classification based on Si content and $Mg/(Mg + Fe^{+2})$ reveals intermediate composition between ferrotschermakite–ferrohornblende[40] and the classification scheme based on $(Al^{VI} + Fe^{+3} + Ti)$ and Al^{IV} content[72] show compositional trends towards pargasite–edenite in MG and DG. The Al content in hornblende geobarometer proposed by Schmidt[73] is used to estimate the pressure during crystallization of granitic pluton. The estimated pressure ranges from 2.07 to 3.58 kb for MG and 4.59 to 8.52 kb for DG, which is consistent with the previous study[40]. Calculation using Al-in-hornblende geobarometry reveals that MG is emplaced at the upper portion (~8 km depth) and DG at a relatively deeper portion (~20 km depth) of the continental crust.

Ti-in-biotite geothermometry

Biotites and co-existing mineral grains are important for textural equilibrium but may not necessarily imply attained equilibrium composition[74]. However, it is assumed that biotite composition attains chemical equilibrium with coexisting phases involving exchange and substitution of elements[64]. In MG and DG, biotites co-exist with apatites and are mostly of magmatic origin, occurring with minerals like quartz, K-feldspar and titanite. This assemblage is sensitive for application of Ti-in-biotite geothermometry. Calculation indicates that biotites are re-equilibrated with associated mineral assemblages within the temperature range of 490–600°C in the Palaeoproterozoic granitoids of central India.

Apatite–biotite equilibria

Apatite is a minor but ubiquitous mineral in granitoids because of its low solubility in silicate melts and limited ability of common rock-forming minerals to accept phosphorus in their structure from granitic magma[10]. It can also accommodate significant amounts of halogen[3] and rare earth elements[10] apart from its importance as a P repository. Halogen (F and Cl) content in apatites can be interpreted as dissolved halogens in the granitic melts and co-existing biotite phases permit F–Cl–OH partitioning

Figure 6. FeO–Fe$_2$O$_3$–TiO$_2$ ternay system of Buddington and Lindsley[60] showing the major solid solution series magnetite–ulvospinel, hematite–ilmenite and pseudobrookite–ferropseudobrookite series in mole per cent. Solid diamond shows the composition of ilmenite and open circle for composition of magnetite from DG with respect to geological processes responsible for oxidation of titanomagnetite to titanohematite. Bold line – titanomahemites.

because of reciprocal mixing properties[75]. Biotite–apatite thermometer grid corroborates with near-liquidus to near-solidus condition ranging from 900°C to 1000°C as well as increased fugacity ratio $\log(f_{H_2O}/f_{HF})$ in crustal melt during crystallization of MG and DG. Apatites with high La, Ce and Nd content in these two granitoids indicate that they control a major portion of REE budget during crystallization of magma. In MG, texturally identifiable core in apatite is an evidence of partial dissolution dominated by magma mixing at the early stage of progressive crystallization. The temperature range of 900 to 1000°C estimated from apatite–biotite equilibria and pressure obtained from amphibole geobarometry (2.0 to 3.5 kb for MG and 4.5 to 8.5 kb for DG) is inferred to be the most probable P–T conditions for magma mixing processes that take place in the Palaeoproterozoic granitoids. Uniform composition along apatite zones indicates that later growth occurred in a relatively static environment with homogeneous melt composition[69].

Accessory mineral saturation

Most commonly occurring accessory phases like apatites, zircons and titanites in granitic magmas seem to be rich in P, Zr and Ti respectively, which behave as incompatible elements in the host rock[4,5,10]. The behaviour of P, Zr, Ti and rare-earth elements (REE) controls the equilibria between accessory minerals and granitic magma during crustal melting[1]. A good understanding of factors controlling accessory mineral crystallization is a fundamental issue in granite petrogenesis[76]. Solubility of accessory minerals is useful for estimation of their saturation temperature in granitic magma.

Apatite saturation

Apatite solubility is useful in understanding the P-budget in granitic magma and estimating saturation temperature. P-content in granitic magma is an accurate measure of temperature of apatite crystallization[10]. Temperature calculations were made using the apatite solubility models proposed by Harrison and Watson[1]. For MG, the available bulk-rock geochemical data[40,41,77,78] is used to estimate the apatite saturation temperature of 806–980°C for rock composition with SiO$_2$ = 60.07–76.74 wt% and P$_2$O$_5$ = 0.02–0.32 wt% (Supplementary Table 10). For DG, the bulk-rock geochemical data[40,42] is used to calculate the apatite saturation temperature range of 753–941°C for rock composition with SiO$_2$ = 66.19–72.73 wt% and P$_2$O$_5$ = 0.01–0.13 wt% (Supplementary Table 10). Temperature calculation shows that the beginning and end of crystallization of apatites is at relatively higher temperature in MG (~980°C) along with significant variation in SiO$_2$ as compared to DG (~940°C) (Figure 7 *a*).

Zircon saturation

Experimental studies demonstrate that low solubility of zircon in crustal melts helps to constrain the temperature at which it is crystallized and the amount of Zr required to achieve the completely saturated condition of the granitic magma[5,79]. Zircon solubility depends on the temperature and composition of granitic magma[79], which is widely used to estimate the zircon saturation temperature. Zircon saturation thermometer is highly accurate for practical applications because of limited analytical errors in Zr, major-element composition and presence of zircon inheritance[6]. Zircon thermometry yields a temperature range of 703–919°C for MG and 834–987°C for DG[80], which corresponds to Zr concentrations ranging from 25 to 291 ppm and 93 to 494 ppm respectively (taken from earlier studies for MG[40,41,77,78] and DG[40,42]). Temperature estimation shows that crystallization of zircon started at relatively lower temperature in MG (~919°C) as compared to DG (~987°C), which continued for a wide temperature range and finally ended at further lower temperature (Figure 7 b).

Titanite saturation

Experimental studies suggest that Ti-solubility in melts decreases as melts become more felsic and strongly depends on temperature and melt composition[81,82]. Ti saturation in magma with high Ca-activities preclude the formation of titanite because of calcic composition and its stability is strongly controlled by the conditions of crystallization and bulk composition[7,8]. Titanites occur as the principal Ti-rich phase in MG and DG indicating that the magma was saturated with TiO_2. Thus, Ti solubility model[82] is useful for estimation of the Ti saturation temperature. Temperature calculation indicates that granitic magma was saturated with Ti in the temperature range of 642–852°C for MG and 645–790°C for DG[80] corresponding to Ti concentration ranging from 143 to 1760 ppm and 150 to 918 ppm, respectively (taken from earlier studies for MG[40,41,77,78] and DG[40,42]. Estimated Ti saturation temperature indicates that Ti-rich phases started crystallizing at slightly higher temperature in MG (~852°C) as compared to DG (~790°C) and ended at similar temperature conditions (~640°C) (Figure 7 c).

Temperature estimates from accessory mineral saturation models reveal the sequence of crystallization of apatite, zircon and titanite in the Palaeoproterozoic granitoids in central India. In MG, apatite is the earliest phase that started crystallizing at ~980°C followed by zircon (~919°C) and titanite (~852°C). In DG, probably zircon is the earliest phase crystallizing at ~987°C followed by apatite (~941°C) and titanite (~790°C). According to Ryerson and Watons[81], Ti-solubility in magma is inversely dependent on silica content; in other words,

Ti-saturation temperature is relatively lower in more felsic magma. In granitic magma, Ti-solubility is most likely thought to reflect a lack of equilibrium with coexisting phases[53] such as apatite and zircon, which are most likely to be saturated in the early stage of crystallization. Thus, Ti-saturation temperature is relatively lower than that of apatite and zircon saturation temperatures, particularly in case of DG. Pandit and Panigrahi[40] suggested that hornblende–plagioclase crystallized in the temperature range 743–773°C for MG and 725–773°C for DG, which is broadly overlapped by the temperature of titanite formation (MG: 642–852°C and DG: 645–790°C).

However, there are occurrences of Dongargarh equivalent granitoid plutons even much larger in size in Dhanora–Manpur[33] towards south, Madanbera towards west, Kanker–Mainpur towards southeast[83] and other occurrences are located in the adjacent areas of Bastar, Sukma, Sitagaon, Keskal, Darbha, etc. These granitoids are compositionally more varied (granite–granodiorite–monzonite) compared to DG[83]. Thus, the origin of Palaeoproterozoic granitoids and felsic magmatism in central India remains rather obscure and needs further attention.

Discussion

Two distinct intrusive Paleoproterozoic granitoid plutons in central India show evidences of evolving granitic magmatism in a continental rift or extensional or divergent tectonic setting[40]. At the early stage of crystallization, the magma eventually becomes saturated with P and Ti, thus crystallizing apatite and titanite as accessory phases[4]. Early progressive crystallization of Palaeoproterozoic granitoids was dominated by magma mixing and partial dissolution processes with the formation of apatite between near-liquidus to near-solidus temperature (900–1000°C) and increased fugacity ratio $\log(f_{H_2O}/f_{HF})$ followed by a relatively static environment in the magma chamber. Apatites are enriched in common LREE (i.e. La, Ce, Nd) and controlled its budget in the magma during crystallization. Higher halogen content in apatite from MG (F = 3.67–6.38 wt% and Cl <0.12 wt%) compared to DG (F = 1.51–1.86 wt% and Cl <0.02 wt%) indicates that parental granitic magma of MG was comparatively richer in F and Cl content. Abundance of F and Cl in granitic magma may play a potential role as ligands in metal transport[84,85] and in formation of magmatic–hydrothermal ore deposits[86]. Biotite–apatite thermometer grid infers that both granitoids are produced from partial wet melting of crustal protolith.

Two varieties of titanite (magmatic and hydrothermal type) crystallized in the Palaeoproterozoic granitoids because of two distinct geological processes, i.e. magmatic and hydrothermal alteration. There are two possibilities of formation of magmatic titanite, either because of hydration reaction that breaks down amphibole to biotite
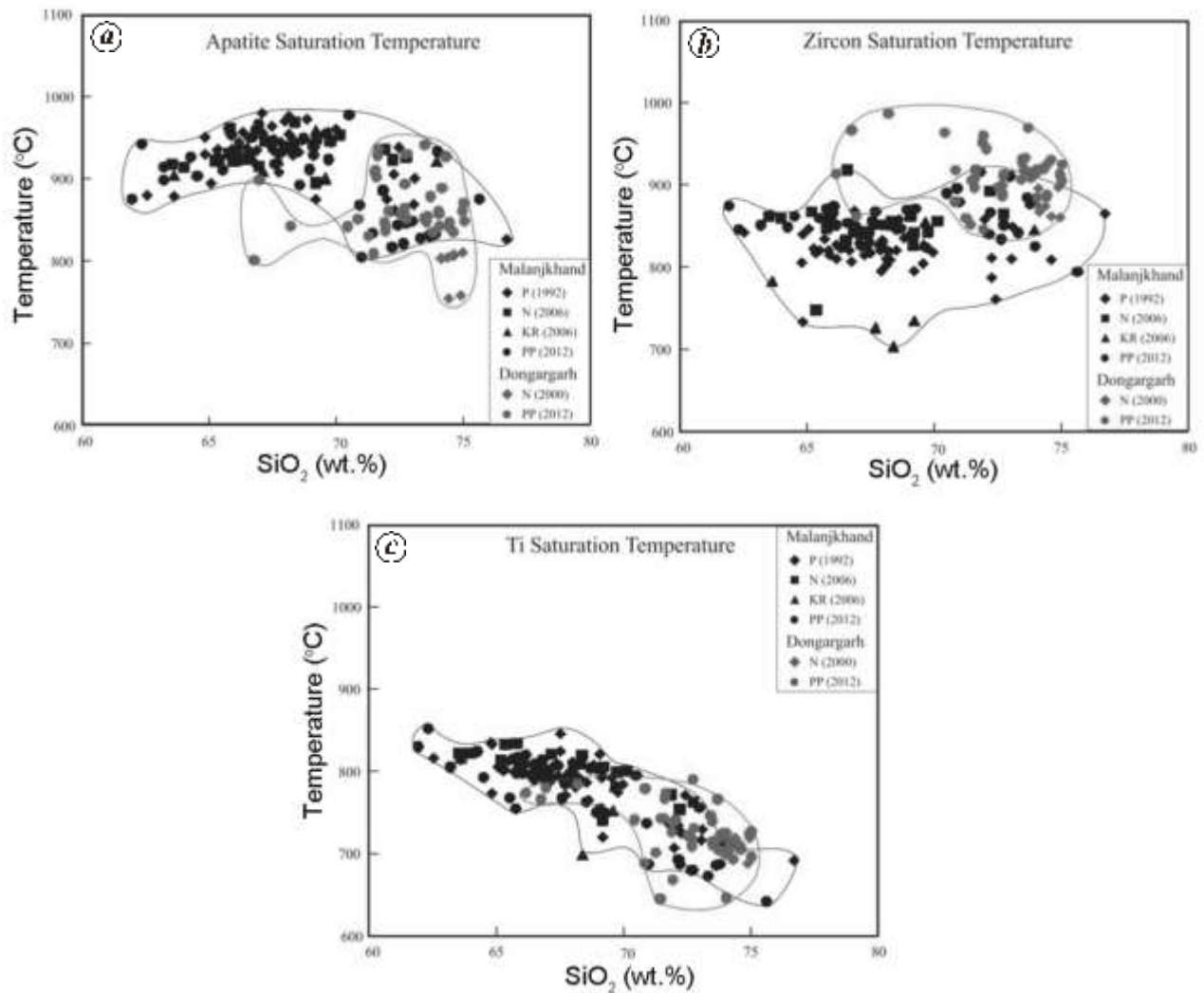
Figure 7. Granite composition (SiO$_2$ wt%) versus estimated temperature for (**a**) apatite, (**b**) zircon and (**c**) Ti-saturation in the parental magma for Malanjkhand and Dongargarh granitoids (Supplementary Table 10).

with a rise in fO$_2$ and fH$_2$O conditions during crystallization of granitic magma or direct crystallization from Ti-saturated granitic melt with high Ca-activities. Presence of oscillatory zoning in magmatic titanite indicates cyclic change in the composition of Ti-saturated granitic magma with crystallization under oxidizing conditions. In DG, titanomagnetite occurs as composite grains (ilmenite and magnetite) in amphiboles and is enclosed by titanite rims with variable width. Possibly, they were re-equilibrated at subsolidus stage at high fO$_2$ conditions close to FMQ buffer, which indicates an oxidized continental crust during the growth of titanite rims around titanomagnetite grains. In MG, hydrothermal titanite formed due to deuteric alteration of Ti-bearing biotite to chlorite, whereas in DG alteration of amphibole to chlorite occurred in presence of titanomagnetite. Formation of hydrothermal titanites and alteration of biotite and amphibole due to hydration reaction suggest high fO$_2$ and

fH$_2$O resulted from late stage hydrothermal activities in the continental crust.

Ti-in-biotite geothermometer infers that biotite attained chemical re-equilibrium during cooling in a temperature range of 490–600°C along with other mineral assemblages, responsible for Ti-substitution. Al-in-hornblende geobarometer estimation indicates that Palaeoproterozoic granitoids in central India emplaced at a pressure of 2–3.5 kb for MG, which is relatively higher for DG than (4.6 to 8.5 kb) corresponding to the middle–upper levels in the continental crust. This result is corroborated with the earlier study by Pandit and Panigrahi[40].

Calculations from the accessory mineral saturation temperature infer two different crystallization sequences of granitic magma for MG and DG. Crystallization sequence of accessory mineral in MG is: apatite → zircon → titanite, whereas that in DG is: zircon → apatite → titanite. Crystallization temperature of titanite

overlaps with the temperature of hornblende-plagioclase formation. Thus, apatite and zircon crystallized earlier than hornblende–plagioclase in the granitic magma forming the two most prominent units of Palaeoproterozoic granitoids in central India.

1. Watson, E. B. and Harrison, T. M., Accessory minerals and the geochemical evolution of crustal magmatic systems: a summary and prospectus of experimental approaches. *Phys. Earth Planet. Int.*, 1984, **35**, 19–30.
2. Robinson, D. M. and Miller, C. F., Record of magma chamber processes preserved in accessory minerals assemblages, Aztec Wash pluton, Nevada. *Am. Mineral.*, 1999, **84**, 1346–1353.
3. Piccoli, P. M., Candela, P. and Rivers, M., Interpreting magmatic processes from accessory phases: titanite – a small scale recorder of large-scale processes. *Trans. R. Soc. Edinb. Earth Sci.*, 2000, **91**, 25–267.
4. Green, T. H. and Adam, J., Pressure effect on Ti- or P-rich accessory mineral saturation in evolved granitic melts with differing K_2O/Na_2O ratios. *Lithos*, 2002, **61**, 271–282.
5. Hanchar, J. M. and Watson, E. B., Zircon saturation thermometry. *Rev. Mineral. Geochem.*, 2003, **53**, 89–112.
6. Miller, C. F., Meschter, S., Dowell, M. and Mapes, R. W., Hot and cold granites? Implication of zircon saturation temperatures and preservation of inheritance. *Geology*, 2003, **31**, 529–532.
7. Troitzsch, U. and Ellis, D. J., The synthesis and crystal structure of $CaAlFSiO_5$, the Al–F analog of titanite. *Am. Mineral.*, 1999, **84**, 1162–1169.
8. Troitzsch, U. and Ellis, D. J., Thermodynamic properties and stability of AlF-bearing titanite $CaTiOSiO_4$–$CaAlFSiO_4$. *Contrib. Mineral. Petrol.*, 2002, **142**, 543–563.
9. Tropper, P., Manning, C. E. and Essene, E. J., The substitution of Al and F in titanite at high pressure and temperature: experimental constraints on phase relations and solid solution properties. *J. Petrol.*, 2002, **43**, 1787–1814.
10. Piccoli, P. M. and Candela, P. A., Apatite in Igneous Systems. *Phosphates–Geochemical, Geobiological and Materials Importance. Rev. Mineral. Geochem.*, 2002, **48**, 255–292.
11. Enami, M., Suzuki, K., Liou, J. G. and Bird, D. K., Al–Fe^{3+} and F–OH substitutions in titanite and constraints on their P–T dependence. *Eur. J. Mineral.*, 1993, **5**, 219–231.
12. Xirouchakis, D. and Lindsley, D. H., Equilibria among titanite, hedenbergite, fayalite, quartz, ilmenite, and magnetite: experiments and internally consistent thermodynamic data for titanite. *Am. Mineral.*, 1998, **83**, 712–749.
13. Broska, I., Harlov, D., Tropper, P. and Siman, P., Formation of magmatic titanite and titanite–ilmenite phase relations during granite alteration in the Tribec Mountains, Western Carpathians, Slovakia. *Lithos*, 2007, **95**, 58–71.
14. Harlov, D., Tropper, P., Seifert, W., Nijland, T. and Forster, H. J., Formation of Al-rich titanite ($CaTiSiO_4O$–$CaAlSiO_4OH$) reaction rims on ilmenite in metamorphic rocks as a function of fH_2O and fO_2. *Lithos*, 2006, **88**, 72–84.
15. Bonamici, C. E., Kozdon, R., Ushikubo, T. and Valley, J. W., Intragrain oxygen isotope zoning in titanite by SIMS: cooling rates and fluid infiltration along the Carthage–Colton Mylonite Zone, Adirondack Moundains, NY, USA. *J. Metamorph. Geol.*, 2014, **32**, 71–92.
16. Ogasawara, Y., Fukasawa, K. and Maruyama, S., Coesite exsolution from supersilicic titanite in UHP marble from the Kokchetav Massif, northern Kazakhstan. *Am. Mineral.*, 2002, **87**, 454–461.
17. Naqvi, S. M. and Rogers, J. J. W., *Precambrian Geology of India*, Oxford University Press, Oxford, 1987.
18. Yedekar, D. B., Jain, S. C., Nair, K. K. K. and Dutta, K. K., The central Indian collision suture. *Geol. Surv. India Spec. Publ.*, 1990, **28**, 1–43.
19. Acharyya, S. K., The nature of Mesoproterozoic Central Indian Tectonic Zone with exhumed and reworked older granulites. *Gondwana Res.*, 2003, **6**, 197–214.
20. Sarkar, S. N., Stratigraphy and tectonics of the Dongargarh System, a new system in the Precambrians of Bhandara – Durg – Balaghat area, Bombay and Madhya Pradesh, Part-I. *J. Sci. Eng. Res.*, 1957–58, **1**, 237–268; **2**, 145–160.
21. Neogi, S., Miura, H. and Hariya, Y., Geochemistry of the Dongargarh volcanic rocks, Central India: implications for the Precambrian mantle. *Precambrian Res.*, 1996, **76**, 77–91.
22. Sensarma, S. and Mukhopadhyay, D., New insight on the stratigraphy and volcanic history of the Dongargarh Belt, Central India. *Gond. Geol. Magz. Spl.*, 2003, **7**, 129–136.
23. Sensarma, S. and Mukhopadhyay, D., Stratigraphy of the ~2.5 Ga Dongargarh belt, Central India: key observations and suggested revisions. *Gond. Geol. Magz. Spl.*, 2014, **16**.
24. Sensarma, S., Hoernes, S. and Mukhopadhyay, D., Relative contributions of crust and mantle to the origin of the Bijli Rhyolite in a palaeoproterozoic bimodal volcanic sequence (Dongargarh Group), central India. *Proc. Indian Acad. Sci. (Earth Planet. Sci.)*, 2004, **113**, 619–648.
25. Chakraborty, T. and Sensarma, S., Shallow marine and coastal eolian quartz arenites in the Neoarchean–Palaeoproterozoic Karutaola Formation, Dongargarh volcanoc-sedimentary succession, central India. *Precambrian Res.*, 2008, **162**, 284–301.
26. Bandyopadhyay, B. K., Roy, A. and Huin, A. K., Structure and tectonics of a part of the central Indian shield. *Geol. Soc. India, Memoir*, 1990, **31**, 433–467.
27. Roy, A., Kagami, H., Yoshida, M., Roy, A., Bandyopadhyay, B. K. and Chattopadhyay, A., Rb/Sr and Sm/Nd dating of different metamorphic events from the Sausar mobile belt, central India: implications for Proterozoic crustal evolution. *J. Asian Earth Sci.*, 2006, **26**, 61–76.
28. Srivastava, R. K. and Gautam, G. C., Precambrian mafic dyke swarms from the southern Bastar Central India craton: present and future perspectives. In *Indian Dykes: Geochemistry, Geophysics, and Geochronology* (eds Srivastava, R. K., Sivaji, C. and Chalapati Rao, N. V.), Narosa Publishing Ltd, New Delhi, 2008, pp. 367–376.
29. Meert, J. G. *et al.*, Precambrian crustal evolution of Peninsular India: A 3.0 billion year odyssey. *J. Asian Earth Sci.*, 2010, **39**, 483–515.
30. Panigrahi, M. K., Naik, R. K., Pandit, D. and Misra, K. C., Reconstructing physico-chemical parameters of hydrothermal mineralization at the Malanjkhand copper deposit, India from mineral chemistry of biotite, chlorite and epidote. *Geochem. J.*, 2008, **42**, 443–460.
31. Panigrahi, M. K., Pandit, D. and Naik, R. K., Genesis of the granitoid affiliated Paleoproterozoic copper-molybdenum deposit at Malanjkhand: a review of status. In *Magmatism, Tectonism and Mineralization* (ed. Kumar, S.), Macmillan Publisher Ltd, India, 2009, pp. 265–292.
32. Panigrahi, M. K., Pandit, D., Moriyama, T. and Ishihara, S., Paleoproterozoic granite-ore systems in the perspective of crustal evolution: insights from the Malanjkhand copper deposit and surrounding granitoids in the Central Indian craton. In *Smart Science for Exploration and Mining: Proc. Soc Geol Applied to Mineral Deposits* (eds William, P. J. *et al.*), Townsville Australia, 2009, vol. 2, pp. 957–959.
33. Pandit, D., Panigrahi, M. K., Moriyama, T. and Ishihara, S., Comparative geochemical, magnetic susceptibility, and fluid inclusion studies on the Paleoproterozoic Malanjkhand and Dongargarh granitoids, Central India and implications to metallogeny. *Mineral. Petrol.*, 2014, **108**, 663–680.

34. Pandit, D., Panigrahi, M. K. and Moriyama, T., Constrains from magmatic and hydrothermal epidotes on crystallization of granitic magma and sulfide mineralization in Paleoproterozoic Malanjkhand granitoid, Central India. *Chem. Erde-Geochem.*, 2014, **74**, 715–733.

35. Pandit, D., Geochemistry of feldspar intergrowth microtextures from Paleoproterozoic granitoids in Central India: implications to exsolution processes in granitic system. *J. Geol. Soc. India*, 2015, **85**, 163–182.

36. Pandit, D., Thermodynamic model for hydrothermal sulfide deposition in the Paleoproterozoic granite ore system at Malanjkhand, India. *Indian J. Geomar. Sci.*, 2015, **44**(11), 1697–1711.

37. Pandit, D., Chloritization in Paleoproterozoic granite ore system at Malanjkhand, Central India: mineralogical studies and mineral fluid equilibria modelling. *Curr. Sci.*, 2014, **106**, 565–581.

38. Pandit, D., A comparative study of the Paleoproterozoic Malanjkhand and Dongargarh granitoids Central India: Implications to crustal evolution and metallogeny, Ph D thesis, Indian Institute of Technology Kharagpur, India, 2008.

39. Pandit, D., Lattice preferred orientation analysis of deformed quartz: an advanced application of high resolution X-ray diffractometer. *J. Geol. Soc. India*, 2012, **79**, 169–174.

40. Pandit, D. and Panigrahi, M. K., Comparative petrogenesis and tectonics of Paleoproterozoic Malanjkhand and Dongargarh granitoids, Central India. *J. Asian Earth Sci.*, 2012, **50**, 14–26.

41. Kumar, S. and Rino, V., Mineralogy and geochemistry of microgranular enclaves in Palaeoproterozoic Malanjkhand granitoids, central India: evidence of magma mixing, mingling, and chemical equilibration. *Contrib. Mineral. Petrol.*, 2006, **152**, 591–609.

42. Narayana, B. L., Mallikharjuna, J., Subba Rao, M. V., Murthy, N. N. and Divakara Rao, V., Geochemistry and origin of Early Proterozoic Dongargarh Rapakavi Granite complex, Central India, an example for magma mixing and differentiation. *Gondwana Res.*, 2000, **3**, 507–520.

43. Kumar, S., Rino, V. and Pal, A. B., Field evidence of magma mixing from microgranular enclaves hosted in Palaeoproterozoic Malanjkhand granitoids, Central India. *Gondwana Res.*, 2004, **7**, 539–548.

44. Sarkar, S. C., Kabiraj, S., Bhattacharya, S. and Pal, A. B., *Nature*, origin and evolution of the granitoid-hosted early Proterozoic copper–molybdenum mineralization at Malanjkhand, central India. *Miner. Deposita*, 1996, **31**, 419–431.

45. Pandit, D., Panigrahi, M. K. and Naik, R. K., Fluid characteristics in the leucogranite phase of the Malanjkhand Granitoid Complex: implications to copper–molybdenum mineralization. In Proceedings of Asian Current Research on Fluid Inclusions (ACROFI-2), 2008, pp. 144–146.

46. Sensarma, S., A bimodal large igneous province and the plume debate: the Paleoproterozoic. *Geol. Soc. Am. Spec. Paper*, 2007, **430**, 831–839.

47. Sensarma, S., Hoernes, S. and Mukhopadhyah, D., Relative contribution of crust and mantle to the origin of the Bijli Rhyolite in a palaeoproterozoic bimodal volcanic sequence (Dongargarh Group), central India. *Proc. Indian Acad. Sci. (Earth Planet. Sci.)*, 2004, **113**, 619–648.

48. Srivastava, R. K., Global intracratonic boninite–norite magmatism during the Neoarchean–Paleoproterozoic: evidence from the Central Indian Bastar Craton. *Int. Geol. Rev.*, 2008, **50**, 61–74.

49. Chalapathi Rao, N. V. and Srivastava, R. K., A new find of boninite dyke from the Paleoproterozoic Dongargarh Supergroup: inference for a fossil subduction zone in the Archaean of the Bastar craton, Central India. *Neues Jb. Miner. Abh.*, 2009, **186**, 271–282.

50. Naganjaneyulu, K. and Santosh, M., The Central Indian Tectonic Zone: a geophysical perspective on continental amalgamation along a Mesoproterozoic suture. *Gondwana Res.*, 2010, **18**, 547–564.

51. Kumar, S., Rino, V., Hayasaka, Y., Kimura, K., Raju, S., Terada, K. and Pathak, M., Contribution of Columbia and Gondwana Super continent assembly- and growth-related magmatism in the evolution of the Meghalaya Plateau and the Mikir Hills, Northeast India: constraints from U–Pb SHRIMP zircon geochronology and geochemistry. *Lithos*, 2017, **277**, 356–375.

52. Gromet, L. P. and Silver, L. T., Rare earth element distribution among minerals in a granodiorite and their petrogenetic implications. *Geochim. Cosmochim. Acta*, 1983, **47**, 925–940.

53. McLeod, G. W., Dempster, T. J. and Faithfull, J. W., Deciphering magma-mixing processes using zoned titanite from the Ross of Mull Granite, Scotland. *J. Petrol.*, 2011, **52**, 55–82.

54. Mitchell, R. S., Pseudomorphs of anatase after sphene from Roanoke County, Virginia. *Am. Mineral.*, 1964, **49**, 1136–1139.

55. Shore, M. and Fowler, A. D., Oscillatory zoning in minerals: a common phenomenon. *Can. Mineral.*, 1996, **34**, 1111–1126.

56. Watson, E. B. and Liang, Y., A simple model for sector zoning in slowly grown crystals: implications for growth rate and lattice diffusion, with emphasis on accessory minerals in crustal rocks. *Am. Mineral.*, 1995, **80**, 1179–1187.

57. Chakhmouradian, A. R., Reguir, E. P. and Mitchell, R. H., Titanite in carbonatitic rocks: genetic dualism and geochemical significance. *Period. Mineral.*, 2003, **72**, 107–113.

58. Panigrahi, M. K. and Mookherjee, A., The Malanjkhand copper (+molybdenum) deposit, India: mineralization from a low – temperature ore – fluid of granitoid affiliation. *Miner. Deposita*, 1997, **32**, 133–148.

59. Panigrahi, M. K., Pandit, D., Naik, R. K. and Ishihara, S., Reconstruction of physicochemical environment of hydrothermal mineralization at Malanjkhand copper deposit, Central India: constraints from sulfur isotope ratios in pyrite, molybdenite and chalcopyrite. *Resour. Geol.*, 2013, **63**, 110–116.

60. Buddington, A. F. and Lindsley, D. H., Iron-titanium oxide mineral and synthetic equivalents. *J. Petrol.*, 1964, **5**, 310–357.

61. Yavuz, F., A revised program for microprobe-derived amphibole analysis using the IMA rules. *Comput. Geosci.*, 1999, **25**, 909–927.

62. Martin, R. F., Amphiboles in the igneous environment. *Rev. Mineral. Geochem.*, 2007, **67**, 323–358.

63. Henry, D. J., Guidotti, C. V. and Thomson, J. A., The Ti-saturation surface for low-to-medium pressure metapelitic biotites: implications for geothermometry and Ti-substitution mechanisms. *Am. Mineral.*, 2005, **90**, 316–328.

64. Henry, D. J. and Guidotti, C. V., Ti in biotite from metapelitic rocks: temperature effects, crystallochemical controls and petrologic applications. *Am. Mineral.*, 2002, **87**, 375–382.

65. Tacker, R. C. and Stormer Jr, J. C., A thermodynamic model for apatite solid solution, application to high-temperature geologic problems. *Am. Mineral.*, 1989, **74**, 877–888.

66. Sallet, R., Fluorine as a tool in the study of quartz bearing magmatic associations: applications of an improved F–OH biotitea patite thermometer grid. *Lithos*, 2000, **50**, 241–253.

67. Harrison, T. M. and Watson, E. B., The behavior of apatite during crustal anatexis: equilibrium and kinetic considerations. *Geochim. Cosmochim. Acta*, 1984, **48**, 1467–1477.

68. Wass, Y., Hendersoon, P. and Elliott, C. J., Chemical homogeneity and metasomatism in the upper mantle: evidence from rare earth and other elements in apatite-rich xenoliths in basaltic nodules from eastern Australia. *Philos. Trans. R. Soc. London*, 1980, **A297**, 333–346.

69. Dempster, T. J., Jolivet, M., Tubrett, M. N. and Braithwaite, C. J. R., Magmatic zoning in apatite: a monitor of porosity and permeability change in granites. *Contrib. Mineral. Petrol.*, 2003, **145**, 568–577.

70. Paterson, B. A., Stephens, W. E. and Herd, D. A., Zoning in granitoid accessory minerals as revealed by backscattered electron imagery. *Mineral. Mag.*, 1989, **53**, 55–61.

71. Wones, D. R., Significance of the assemblage titanite + magnetite quartz in granitic rocks. *Am. Mineral.*, 1989, **74**, 744–749.

72. Deer, W. A., Howie, R. A. and Zussman, J., *An Introduction of the Rock – Forming Minerals*, Longman Group, London, 1979.

73. Schmidt, M. W., Amphibole composition in tonalite as a function of pressure: an experimental calibration of the Al-in-hornblende barometer. *Contrib. Mineral. Petrol.*, 1992, **110**, 304–310.

74. Guidotti, C. V., Teichmann, F. and Henry, D. J., Chlorite-bearing polymetamorphic metapelites in the Rangeley area, Maine: evidence from equilibrium assemblages. *Am. Mineral.*, 1991, **76**, 867–879.

75. Zhu, C. and Sverjensky, D. A., F–Cl–OH partitioning between biotite and apatite. *Geochim. Cosmochim. Acta*, 1992, **56**, 3435–3467.

76. Hoskin, P. W. O., Kinny, P. D., Wyborn, D. and Chappell, B. W., Identifying accessory mineral saturation during differentiation in granitoid magmas: an integrated approach. *J. Petrol.*, 2000, **41**, 1365–1396.

77. Panigrahi, M. K., Copper–molybdenum mineralization and associated granitoids of Malanjkhand, MP, India, Ph D thesis, Indian Institute of Technology Kharagpur, India, 1992.

78. Naik, R. K., The Late Archean/Early Proterozoic granitoid complex and associated Cu–Mo mineralization at Malanjkhand, Central India: towards working model of ore genesis. Ph D thesis, Indian Institute of Technology Kharagpur, India, 2006.

79. Watson, E. B. and Harrison, T. M., Zircon saturation revisited: temperature and composition effects in a variety of crustal magma types. *Earth Planet. Sci. Lett.*, 1983, **64**, 295–304.

80. Pandit, D., Accessory minerals in Paleoproterozoic granites of Bastar Craton. In National Conference and Field Workshop on Precambrians of India, Society of Earth Scientists India, Jhansi, 2016, pp. 32–33.

81. Ryerson, F. J. and Watson, E. B., Rutile saturation in magmas: implication for Ti–Nb–Ta depletion in island-arc basalts. *Earth Planet. Sci. Lett.*, 1987, **86**, 225–239.

82. Hyden, L. A. and Watson, E. B., Rutile saturation in hydrous siliceous melts and its bearing on Ti-thermometry of quartz and zircon. *Earth Planet. Sci. Lett.*, 2007, **258**, 561–568.

83. Sarkar, S. C. and Gupta, A., Crustal evolution and metallogeny in India, Cambridge University Press, Cambridge, Great Britain, 2012.

84. Holland, H. D., Granite, solutions, and base metal deposits. *Econ. Geol.*, 1972, **67**, 281–301.

85. Candela, P. A. and Holland, H. D., A mass transfer model for copper and molybdenum in magmatic hydrothermal system: the origin of porphyry-type Ore deposits. *Econ. Geol.*, 1986, **81**, 1–19.

86. William-Jones, A. E. and Heinrich, C. A., Vapor transport of metals and the formation of magmatic-hydrothermal ore deposits. *Econ. Geol.*, 2005, **100**, 1287–1312.

87. Jain, S. C., Nair, K. K. and Yedekar, D. B., Geology of Son-Narmada–Tapti lineament zone of Central India. *Geol. Surv. India Spec. Publ.*, 1995, **10**, 1–154.

88. Whitney, D. L. and Evans, B. W., Abbreviations for names of rock-forming minerals. *Am. Mineral.*, 2010, **95**, 185–187.

89. Lepage, L. D., ILMAT: an Excel worksheet for ilmenite–magnetite geothermometry and geobarometry. *Comput. Geosci.*, 2003, **29**, 673–678.

90. Yavuz, F., Evaluating micas in petrologic and metallogenic aspect: I-definitions and structure of the computer program MICA+. *Comput. Geosci.*, 2003, **29**, 1203–1213.

91. Carmichael, I. S. E., The iron-titanium oxides of salic volcanic rocks and their associated ferromagnesian silicates. *Contrib. Mineral. Petrol.*, 1967, **14**, 36–64.

92. Yavuz, F., BIOPAG-PC: Program for an apatite and biotite geothermometer. *Comput. Geosci.*, 1998, **24**, 885–891.